Molecular Microbiology (2008) 70(4), 837–852 ■
doi:10.1111/j.1365-2958.2008.06448.x
First published online 3 October 2008

Actin-depolymerizing factor, ADF/cofilin, is essentially required in assembly of *Leishmania* flagellum

T. V. Satish Tammana,[1†] Amogh A. Sahasrabuddhe,[1†] Kalyan Mitra,[2] Virendra K. Bajpai[2] and Chhitar M. Gupta[1*]
[1]*Division of Molecular and Structural Biology and*
[2]*Electron Microscopy Unit, Central Drug Research Institute, Lucknow 226001, India.*

Summary

ADF/cofilins are ubiquitous actin dynamics-regulating proteins that have been mainly implicated in actin-based cell motility. Trypanosomatids, e.g. *Leishmania* and *Trypanosoma*, which mediate their motility through flagellum, also contain a putative ADF/cofilin homologue, but its role in flagellar motility remains largely unexplored. We have investigated the role of this protein in assembly and motility of the *Leishmania* flagellum after knocking out the ADF/cofilin gene by targeted gene replacement. The resultant mutants were completely immotile, short and stumpy, and had reduced flagellar length and severely impaired beat. In addition, the assembly of the paraflagellar rod was lost, vesicle-like structures were seen throughout the length of the flagellum and the state and distribution of actin were altered. However, episomal complementation of the gene restored normal morphology and flagellar function. These results for the first time indicate that the actin dynamics-regulating protein ADF/cofilin plays a critical role in assembly and motility of the eukaryotic flagellum.

Introduction

Eukaryotic cilia and flagella are highly conserved organelles that are required in diverse motile and sensory functions (Afzelius, 2004; Snell *et al.*, 2004; Pan *et al.*, 2005; Quarmby and Parker, 2005). The flagellum of trypanosomatids, such as *Trypanosoma* and *Leishmania*, is a unique multifunctional organelle that plays critical roles in cell motility, chemotaxis, cell signalling and host cell invasion (Landfear and Ignatushchenko, 2001; Gull, 2003; Hill, 2003; Kohl, 2003) and is comprised of two main components, the axoneme and paraflagellar rod (PFR). The axoneme is composed of around 250 proteins arranged in a core structure of nine peripheral microtubule doublets surrounding two single microtubules (Ralston and Hill, 2008). In addition, these organisms contain a unique crystalline lattice structure, called PFR, running along the axoneme under the flagellar membrane (Maga and Lebowitz, 1999). While the canonical 9 + 2 axoneme structure powers beating in most eukaryotic flagella (Ralston and Hill, 2008), PFR has been implicated in flagellar motility and waveform generation (Maga and Lebowitz, 1999). A number of studies have shown that microtubule-based dynein and kinesin motors play pivotal role in dynamic assembly and motility of the trypanosomatid flagellum (Blaineau *et al.*, 2007; Absalon *et al.*, 2008; Ralston and Hill, 2008). However, despite their presence in the flagellum of various organisms including *Leishmania* (Muto *et al.*, 1994; Yanagisawa and Kamiya, 2001; Sahasrabuddhe *et al.*, 2004; Minoura, 2005), the role of actin and actin-binding proteins (Ross *et al.*, 2008) still remains largely unexplored.

Actin is a ubiquitous cytoskeletal protein that exists in filamentous (F-) and monomeric (G-) states. In its filamentous state, actin forms a complex network with the help of a variety of actin-binding proteins (Sheterline and Sparrow, 1994). The dynamics of this network is regulated by a specific group of actin-binding proteins of which actin-depolymerizing factor ADF/cofilin constitutes an important component (Ono, 2007). ADF/cofilins are essentially present in all eukaryotic cells and have been suggested to play a key role in actin-based cell motility (Pollard and Borisy, 2003).

Leishmania are an important group of parasites that cause a spectrum of human diseases including 'kala-azar', and have been exploited as a model system to explore the mechanisms that regulate flagellar assembly and motility in eukaryotic organisms. Here we show that deletion of the ADF/cofilin gene in *Leishmania* results in immotile cells with reduced flagellar length and severely impaired beat. Additionally, the PFR is not made, vesicle-like structures appear throughout the flagellum and actin distribution is markedly altered. These results strongly suggest that the actin dynamics-regulating protein, ADF/cofilin, plays a crucial role in flagellar assembly and motility.

Accepted 29 August, 2008. *For correspondence. E-mail drcmg@rediffmail.com; Tel. (+91) 522 2610282; Fax (+91) 522 2623405. †Equal contribution.

Results

Expression, intracellular distribution and biochemical characterization of Leishmania *ADF/cofilin (LdCof)*

ADF/cofilin family of proteins are small-molecular-weight actin-binding proteins that depolymerize F-actin into actin monomers and consequently increase the turnover of actin filaments (Dos Remedios *et al.*, 2003; Ono, 2007). In addition, these proteins exhibit actin filament-severing activity that generates new barbed ends and facilitates a rapid increase in filament assembly (Ono, 2007). Besides the actin filament-depolymerizing and -severing activities, ADF/cofilins have also been implicated in the treadmilling process due to their ability to increase the rate of actin filament turnover in steady-state F-actin solutions (Ono, 2007).

LdCof was cloned, overexpressed with His_6 at its C-terminus and purified to homogeneity (Fig. 1A). The molecular identity of the purified recombinant LdCof (rLdCof) was confirmed by sequencing a portion of its N-terminus (AISGVTLEENV) and also by mass spectrometry (molecular mass 16 920 Da). Monospecific anti-rLdCof antibodies were prepared by separately immunizing both rabbits and mice with rLdCof followed by affinity purification of the antisera. These antibodies recognized a 17 kDa protein in lysates of various *Leishmania* species, confirming the expression of LdCof in these parasites (Fig. 1B). The intracellular distribution of LdCof was determined by immunofluorescence microscopy using anti-rLdCof antibodies as well as by overexpression of LdCof as its GFP fusion in *Leishmania* promastigotes (Fig. 1C; also see Fig. S1). This protein was present throughout the cell body including the flagellum, but its concentration was relatively higher in the anterior region including the flagellar base.

Actin-depolymerizing activity of rLdCof was determined by the pelleting assay (Ono and Benian, 1998) using rabbit muscle actin (actin) and *Leishmania* actin (LdACT) as substrates and recombinant human cofilin (rHCof) as a control (Fig. 2A–C). Similar to rHCof, rLdCof depolymerized both actin and LdACT filaments, but it co-pelleted only with LdACT filaments. As ADF/cofilin interactions with actin have been shown to be pH-dependent (Hawkins *et al.*, 1993; Blondin *et al.*, 2002), we analysed the effects of pH on both the actin binding and depolymerization activities of rLdCof by the pelleting assay at a range of pH 6.0–9.0 (Fig. 2D). Unlike rHCof, no change was observed in both the actin binding and actin depolymerization

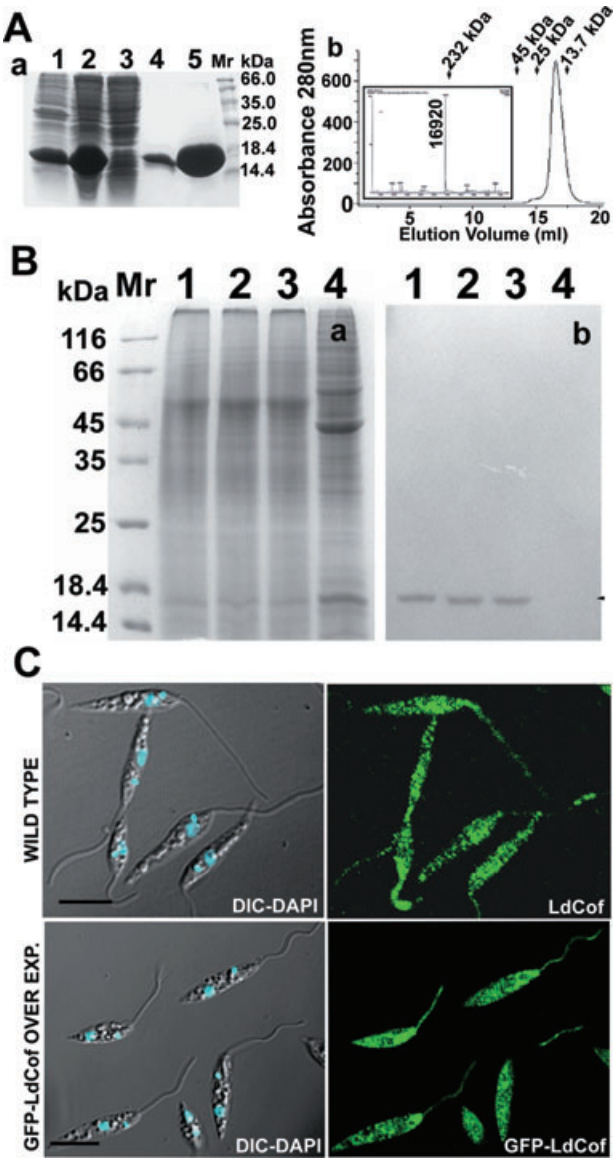

Fig. 1. A. Characterization of recombinant *Leishmania* ADF/cofilin containing His_6 at its C-terminus (rLdCof). (a) Coomassie blue-stained SDS-PAGE of rLdCof overexpression induced in BL21 (DE3) cells. Lane1, pellet fraction; lane 2, soluble fraction; lane 3, Ni-NTA Sepharose column passthrough; lane 4, column wash; lane 5, eluate containing pure rLdCof; Mr, molecular weight markers. (b) Size exclusion chromatograph showing monomeric nature of rLdCof. Arrows mark peak positions of the marker proteins, namely catalase (232 kDa), ovalbumin (45 kDa), chymotrypsinogen A (25 kDa) and ribonuclease (13.7 kDa). Precise mass of rLdCof (16 920 Da) obtained by electro-spray ionization mass spectrometry is shown in the inset.
B. Expression of LdCof in *Leishmania* species. (a) Coomassie blue-stained 10% SDS-PAGE; (b) Western blot of (a) using rabbit anti-rLdCof antibodies. Mr, molecular weight markers; lane 1, *L. donovani* promastigote lysate; lane 2, *L. major* promastigote lysate; lane 3, *L. tropica* promastigote lysate; lane 4, HepG2 cell lysate. Lanes 1–4 contained 30 μg of protein per lane.
C. Intracellular distribution of LdCof in *L. donovani* promastigotes determined by immunofluorescence microscopy, using mouse anti-rLdCof antibodies and also by fluorescence microscopy of the *L. donovani* promastigotes that overexpressed GFP fusion protein of LdCof (GFP–LdCof) (see Fig. S1). The LdCof distribution was polarized towards the anterior region in > 70% wild type cells and in >80% GFP–LdCof-overexpressing cells. In each case, about 1000 cells were assessed for the LdCof distribution. Bar, 5 μm.

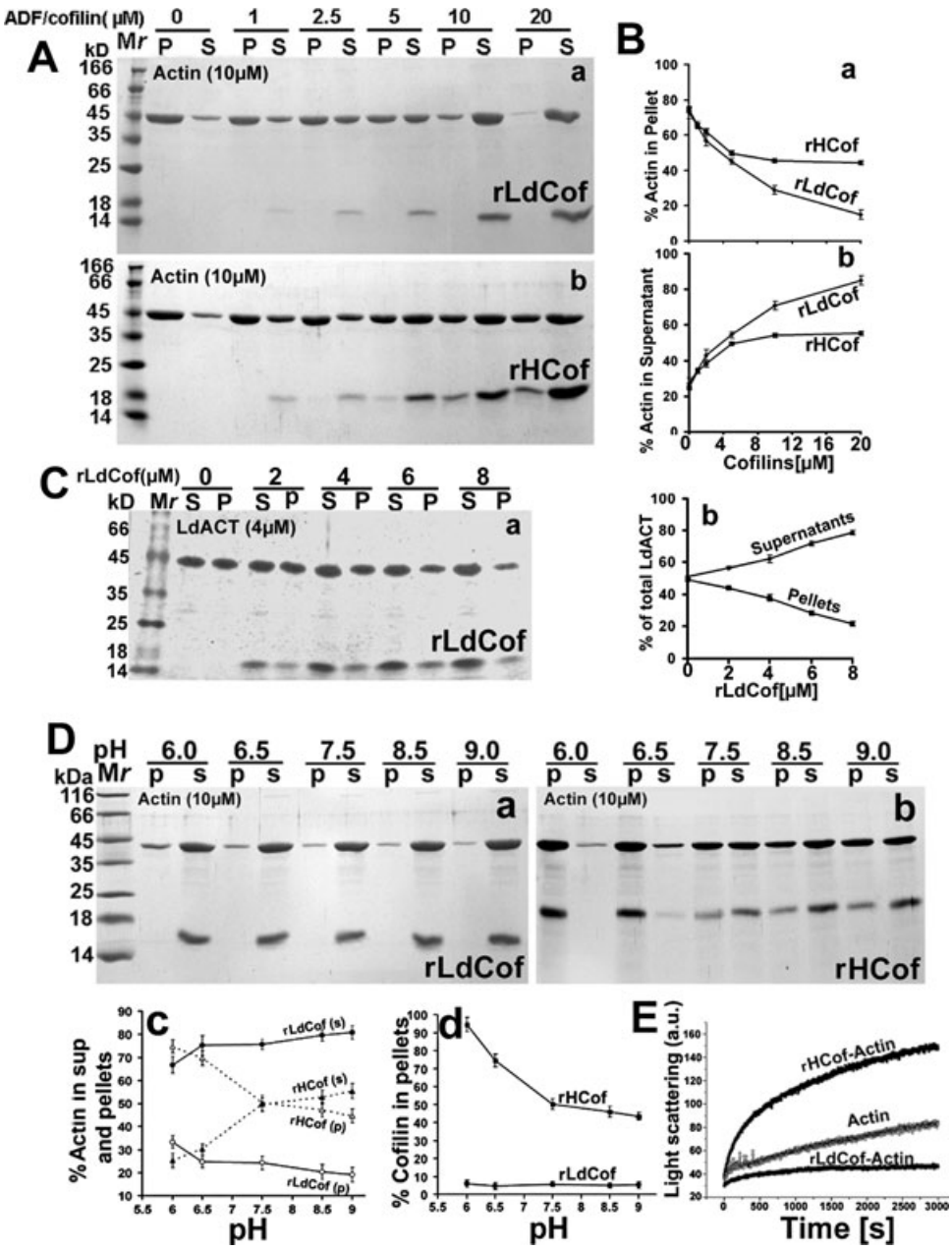

Fig. 2. Depolymerization of rabbit muscle actin (actin) and *Leishmania* actin (LdACT) by rLdCof.
A. Depolymerization of F-actin by rLdCof and rHCof. Coomassie blue-stained SDS-PAGE of supernatant (S) and pellet (P) fractions. rLdCof (a), unlike rHCof (b), did not co-sediment with F-actin at any of its concentrations in identical buffer and pelleting conditions.
B. Quantitative analysis of F-actin depolymerization by rLdCof and rHCof at their varying concentrations. (a) Actin in pellets, (b) actin in supernatants. Values are expressed as percentages of total actin and are means of three independent experiments ± standard deviations.
C. Depolymerization of recombinant *Leishmania* actin (LdACT) by rLdCof. (a) Coomassie blue-stained SDS-PAGE of supernatant (S) and pellet (P) fractions. In contrast to actin, rLdCof co-sedimented readily with the pellet fractions of LdACT. (b) Quantitative analysis of F-LdACT depolymerization by rLdCof at its varying concentrations. Values shown are means of three independent experiments ± standard deviation.
D. Effect of pH on F-actin depolymerization as well as co-sedimentation with rLdCof or rHCof at equimolar concentrations (10 μM each). (a) Coomassie blue-stained gel showing F-actin depolymerization and F-actin binding with rLdCof at varying pH conditions. (b) Coomassie blue-stained gel showing F-actin depolymerization and F-actin binding with rHCof at varying pH conditions. (c) Quantitative analysis of pH-dependent F-actin depolymerization by rLdCof (circles) and rHCof (triangles). Values shown for actin in the soluble (S) and pellet (P) fractions are expressed as percentage of total actin and are means of three independent experiments ± standard deviation. (d) Quantitative analysis of pH-dependent co-sedimentation of rLdCof and rHCof with F-actin (Pellet). Values are expressed as percentages of total rLdCof and rHCof pelleted with F-actin and are means of three independent experiments ± standard deviation.
E. Polymerization of actin.ADP complexed with rLdCof or rHCof at pH 6.5. Polymerization kinetics (by light scattering) of 4 μM complexes in buffer containing 100 mM KCl, 2 mM $MgCl_2$, 1 mM dithiothreitol, 0.5 mM ATP, 0.2 mM $CaCl_2$, 0.5 mM NaN_3, 10 mM Tris-HCl, pH 8.2, when switched to pH 6.5 by addition of 25 mM 2-(morpholino)ethanesulfonic acid.

activities of rLdCof under these conditions. To further confirm these results, we formed complexes of rLdCof (or rHCof) with ADP.actin and induced their polymerization at pH 6.5 (Fig. 2E). rLdCof–ADP.actin complex did not undergo any polymerization, whereas under identical conditions, rHCof–ADP.actin complex polymerized readily, confirming the pH-insensitive behaviour of rLdCof towards F-actin binding and depolymerization. This is consistent with the behaviour of LdACT that polymerizes *in vitro* in a restricted range of pH 7.0–8.5 (Kapoor *et al*., 2008). Besides filamentous actin, ADF/cofilins also bind the monomeric form of actins (Ono, 2007). The binding of LdCof with actin monomers was analysed by the actin depletion pull-down assay (Fig. 3A and B). LdCof effectively bound monomers of both actin and LdACT.

The main physiological function of all ADF/cofilins is to enhance the actin filament turnover and not to completely depolymerize actin (Ono, 2007). The effect of rLdCof on the rate of turnover of actin filaments was monitored by measuring the rate of decrease in fluorescence of ε-ADP-bound F-actin after adding chase amount of ATP (Fig. 3C). Both rLdCof and rHCof increased the rates of turnover of actin filaments with greater enhancement of turnover rate observed with rLdCof, compared with rHCof. Further, the turnover rates were dependent upon rLdCof and rHCof concentrations. Whereas lower concentrations of both the proteins promoted actin treadmilling, higher concentrations appeared to decrease this activity. This is consistent with earlier observations on HCof (Carlier *et al*., 1997).

Besides depolymerization, ADF/cofilins also exhibit actin filament-severing activity, which further promotes actin dynamics. As these proteins lack capping activity in contrast to gelsolins (Dos Remedios *et al*., 2003), each severing event creates a new barbed end that strongly promotes rapid polymerization of actin (Andrianantoandro and Pollard, 2006). To measure the severing activity of rLdCof, we adopted the perfusion assay as described by Ono *et al*. (2004). Actin filaments labelled with TRITC-actin (Molecular Probes, USA) and biotin-actin were attached to streptavidin-coated glass coverslips and observed under a fluorescence microscope. These filaments were stable up to 5 min without any significant change in their morphology, lengths and fluorescence intensity after perfusion of buffer alone. Fluorescence was captured at 1 min intervals up to 5 min after perfusion of different concentrations of rHCof and rLdCof. In both the cases, lengths of actin filaments reduced with time and resulted mostly in dot-like structures (Fig. 4A). However, microscopic analyses of the captured images of actin filaments, treated with rHCof or rLdCof, showed marked differences in their mode of length reduction. Careful examination of the sequential images revealed that rLdCof mostly reduced filament lengths from one

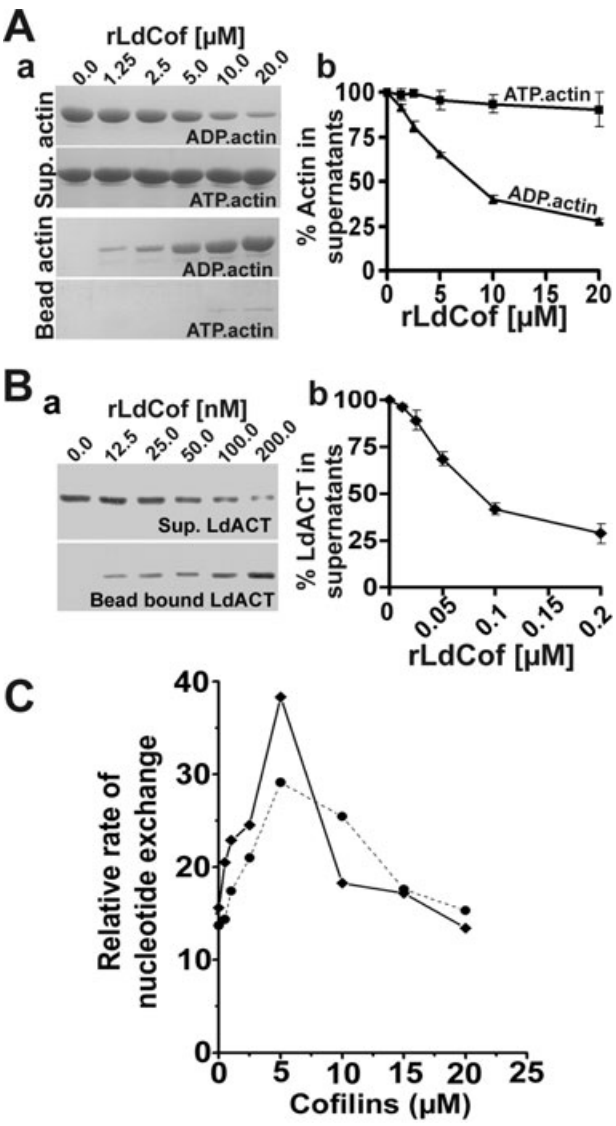

Fig. 3. A. Binding of actin monomers at varying concentrations of rLdCof. (a) Coomassie blue-stained SDS-PAGE of both ADP.actin and ATP.actin in supernatants and bound to Ni-NTA beads. (b) Quantitative analyses of ADP.actin and ATP.actin depletion at various concentrations of rLdCof. Values represent means of three independent experiments ± standard deviation.
B. Binding of rLdCof with LdACT monomers in lysates of LdCof null mutants (1.6 mg protein ml^{-1}) at its varying concentrations. (a) Western blot analyses of LdACT in supernatants and bead-bound form using anti-LdACT antibodies. (b) Quantitative analyses of depletion of LdACT in supernatants. Values shown are means of three independent experiments ± standard deviation.
C. Relative rates of nucleotide exchange at different concentrations of rLdCof and rHCof. The rate of treadmilling (relative rate of nucleotide exchange) was obtained from the decrease in fluorescence of ε-ADP-bound F-actin (15 μM) in F-actin buffer (pH 7.4) in the presence of varying concentrations of rLdCof or rHCof after addition of chase amount of ATP (1 mM) at 20°C. Diamonds, rLdCof; circles, rHCof.

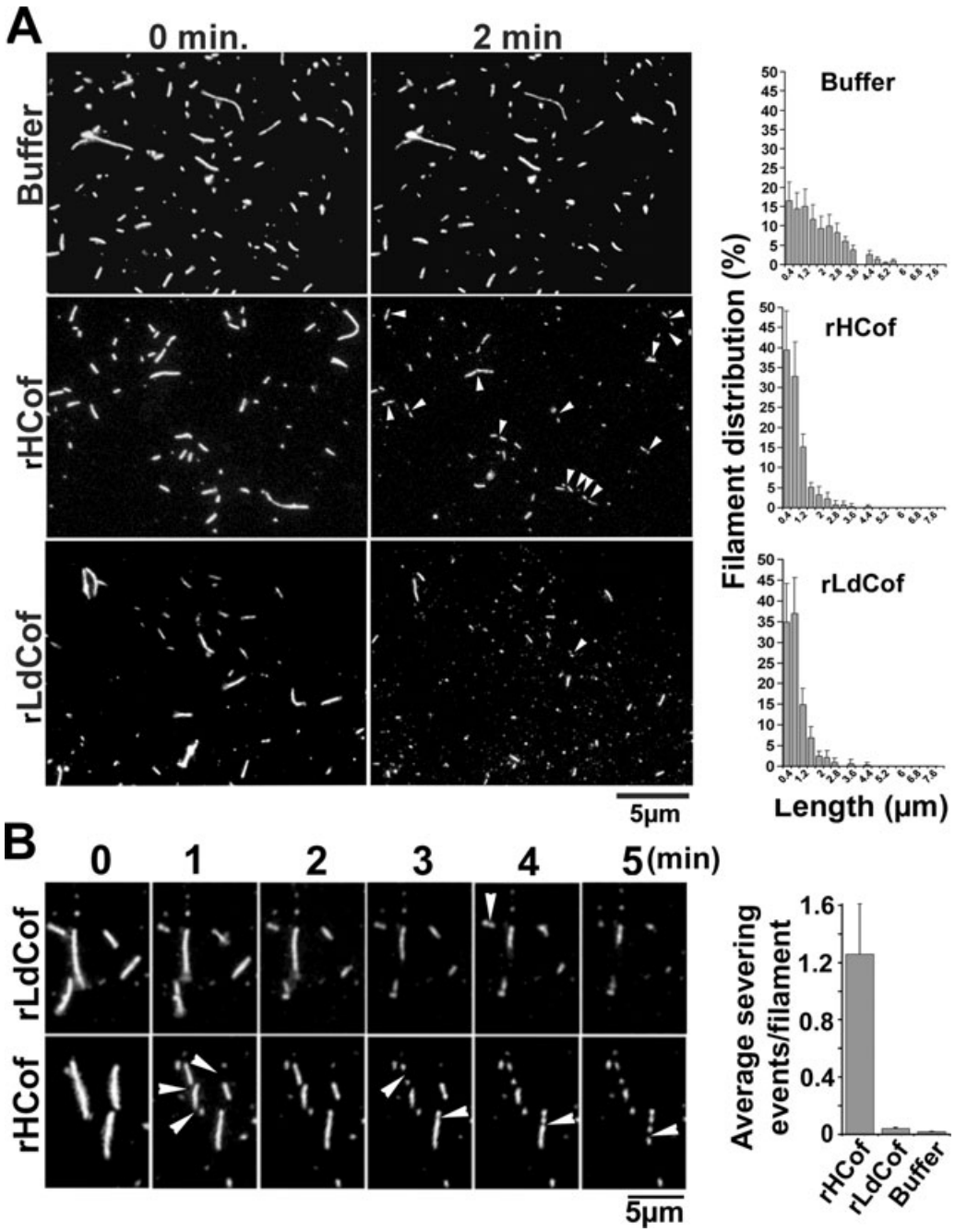

Fig. 4. A. Direct observation of actin filament disassembly by cofilins. Rhodamine/biotin-labelled actin filaments were tethered to glass coverslips through streptavidin and treated with buffer alone, 10 nM rHCof and 10 nM rLdCof. The filaments were observed before and 2 min after the treatment. Bar, 5 μM. Arrow heads mark the visible severing events. Distributions of rhodamine-labelled actin filament lengths were measured in each experiment. Values are expressed as percent distribution of filament length, and are means of five independent experiments ± standard deviation.

B. Microscopic analysis of actin filament severing by cofilins. Sequential time-course images of actin filaments attached through streptavidin on the glass coverslips, after treatment with 10 nM rHCof and 10 nM rLdCof. The magnified images clearly showed visual breaks along the filament, treated with rHCof, whereas such breaks were not noticeable with the filaments that were treated with rLdCof, although the filament lengths were reduced in both the cases. Arrow heads mark the visible severing events. Severing events/filaments were determined by measuring the severing events as visual breaks along the length of actin filaments up to 5 min after treatment with cofilins. Only the filaments that were 2 μM or longer in length in a given field (at least 120 filaments per field) were evaluated in five independent experiments and values are expressed as average number of severing events per filament ± standard deviation.

end and typical severing events were occasional; however, rHCof displayed characteristic patterns of severing events frequently. We therefore also measured the number of severing events as visual breakpoints introduced along the length of filaments versus total number of filaments in a field (Fig. 4B). In order to reduce the chances of error, we only examined the filaments that were 2 μm or longer in length. When compared with rHCof, rLdCof displayed significantly reduced severing activity. The severing activity was also analysed at 10 nM, 100 nM and 1 μM concentrations of cofilins, but no appreciable improvement in the severing activity of rLdCof was observed at any of these concentrations. These results suggest that rLdCof possesses weak actin filament-severing activity.

Generation of LdCof knockout mutants

To understand the function of LdCof in *Leishmania*, we generated *LdCOF* null mutants (*LdCOF*$^{-/-}$) through sequential targeted replacement of the *LdCOF* gene by selective marker genes conferring resistance to neomycin (NEO) and hygromycin B (HYG). Since *Leishmania* is a diploid organism, knocking off the *LdCOF* gene required the replacement of both the alleles of this gene. Gene-targeting constructs were prepared using ~1 kb 5′UTR and ~1 kb 3′UTR of *LdCOF* gene flanking either the hygromycin- or neomycin-resistance markers. Transfection of wild-type *Leishmania* cells with the neomycin-targeting construct and subsequent selection of the transfectants on DMEM agar plates containing 50 μg ml^{-1} G418 resulted by the third week of transfection in stably transfected *Leishmania* clones that were heterozygous for *LdCOF* gene locus (*LdCOF*$^{+/-}$). Several heterozygous clones were proliferated in DMEM liquid cultures and the replacement of one of the *LdCOF* alleles with the *NEO* gene cassette was confirmed by Southern blot analysis. All the clones showed the integration of the *NEO* gene cassette at the ADF/coflin locus. The results of genetic analysis of six such heterozygous clones are presented in Fig. S2.

One of the above-selected heterozygous clones (*LdCOF*$^{+/-}$) was proliferated and subjected to a second round of transfection with the hygromycin-targeting construct. Subsequent selection on DMEM agar plates containing 50 μg ml^{-1} hygromycin B and 50 μg ml^{-1} neomycin resulted in stably transfected homozygous clones (*LdCOF*$^{-/-}$). Several colonies appeared on DMEM agar plates by the third week after transfection, indicating that the selection efficiency of the double-allele replacement was similar to that observed with the heterozygous transfectants. The results of Southern blot analysis of one each of the heterozygous and homozygous clones are given in Fig. 5A and B.

Deletion of the ADF/cofilin gene in Leishmania *promastigotes leads to severe defects in flagellum length, beat and motility*

Microscopic observation of all the homozygous clones revealed that these clones were phenotypically indistinguishable from the heterozygous clones and contained completely immotile populations. Immunoblot analysis of total cell lysates from *LdCOF*$^{+/+}$, *LdCOF*$^{+/-}$ and *LdCOF*$^{-/-}$ cells using anti-LdCof antibodies confirmed the anticipated decrease in the amounts of endogenous LdCof in *LdCOF*$^{+/-}$ mutants and its complete absence in *LdCOF*$^{-/-}$ cells (Fig. 5C; also see Fig. S2).

The *LdCOF*$^{+/-}$ and *LdCOF*$^{-/-}$ cells showed defects in growth (Fig. 5D), motility, flagellar beat and cell shape. The motility and flagellar beat defects of individual cells were monitored by time lapse microscopy and the motility defect of the entire population was assessed by sedimentation assay (Fig. 6A and B; also see Movies S1 and S2). *LdCOF*$^{+/-}$ and *LdCOF*$^{-/-}$ cells were completely immotile and all the cells settled down at the bottom of the culture flask, compared with the fast-moving wild-type promastigotes. Further, the flagella of the heterozygous and the homozygous mutants were paralysed with occasional restricted beating (Fig. S3 and Movies S4 and S5). The typical wave form of flagellar beat was absent. Cell and flagellar morphology were assessed by scanning electron microscopy. The *LdCOF*$^{+/-}$ and *LdCOF*$^{-/-}$ mutants were short and stumpy, as compared with the wild-type cells that were slender and elongated (Fig. 7A). The flagellum of the *LdCOF*$^{+/-}$ and *LdCOF*$^{-/-}$ mutants was approximately four times shorter in length than in the wild-type cells. The average length of the flagellum in *LdCOF*$^{+/-}$ and *LdCOF*$^{-/-}$ mutants was 2.07 ± 1.34 μm ($n = 210$) and 3.09 ± 0.95 μm ($n = 225$) respectively, whereas wild-type cells had an average flagellar length of 12.24 ± 3.85 μm ($n = 215$) (Fig. 7C). Further, unlike the *LdCOF*$^{+/+}$ cells, 'blob-like' structures were observed at the distal tip and at various positions along the length of the flagellum of *LdCOF*$^{+/-}$ and *LdCOF*$^{-/-}$ cells (Fig. 7A and B).

ADF/cofilin is required in assembly of Leishmania *flagellum*

To further study the effect of *LdCOF* deletion on flagellar structure and assembly, we analysed about 50 transverse and longitudinal sections of the *LdCOF*$^{+/+}$, *LdCOF*$^{+/-}$ and *LdCOF*$^{-/-}$ cells by transmission electron microscopy. Unlike the *LdCOF*$^{+/+}$ cells, which showed the presence of PFR running along the axoneme, all sections of the *LdCOF*$^{+/-}$ and *LdCOF*$^{-/-}$ cells were completely devoid of such a structure (Fig. 8A). The absence of PFR in the mutant cells resulted in reduction of the diameter of their flagellum, which appeared circular instead of oval as in

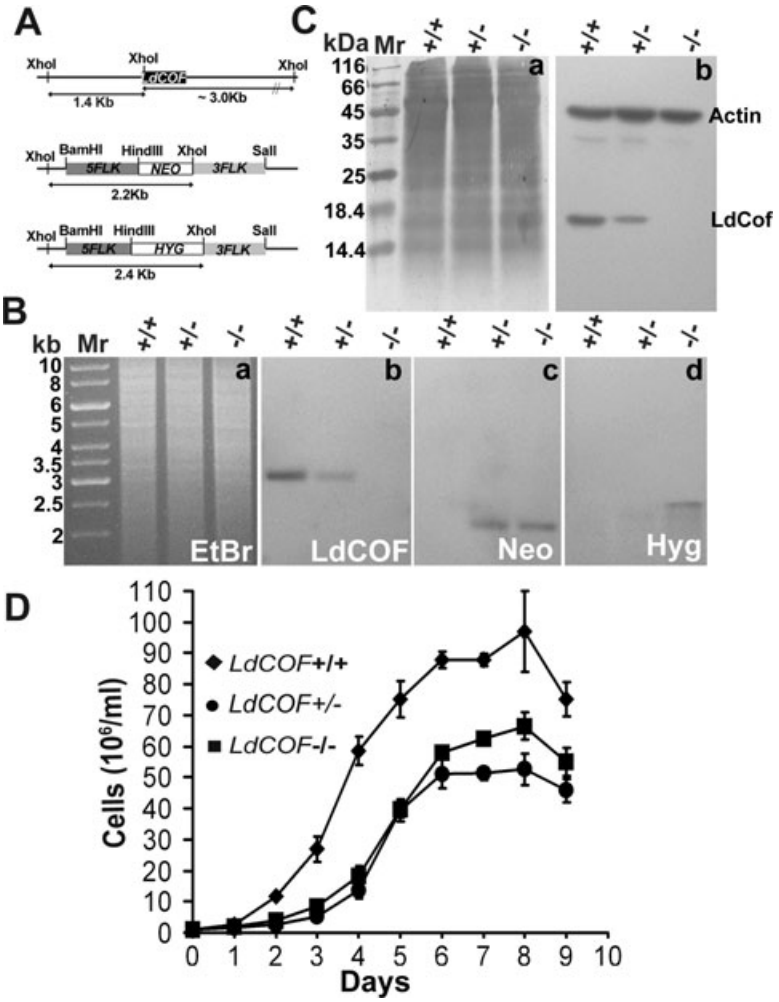

Fig. 5. A. Construction of *LdCof* mutants by homologous recombination. Schematic representation of the *LdCOF* locus in *L. donovani* before and after integration of NEO and/or HYG cassettes, and incorporation of XhoI sites during DNA manipulation. The sizes of XhoI restriction fragments recognized by *LdCOF*, *NEO* and *HYG* probes are shown. 5FLK and 3FLK are 5′ and 3′ flanking DNA sequences respectively, used in the constructs.
B. Southern blot analysis of genomic DNA of *LdCOF*$^{+/+}$ (wild type), *LdCOF*$^{+/-}$ (single-allele knockout) and *LdCOF*$^{-/-}$ (double-allele knockout) cells. (a) Ethidium bromide-stained gel of genomic DNA digested with XhoI. (b), (c) and (d) are Southern blots probed with digoxin-labelled *LdCOF*, NEO and HYG gene probes respectively, showing the replacement of both the *LdCOF* alleles and integration of NEO and HYG gene cassettes. Mr, DNA ladder.
C. Western blot analysis showing depletion of LdCof protein. (a) Coomassie blue-stained 12% SDS-PAGE of total cell lysates showing equal loading of samples. (b) Western blotting of (a) using polyclonal mouse anti-rLdCof antibodies, which detect a specific protein band of about 17 kDa in total cell lysates, and polyclonal rabbit anti-*Leishmania* actin antibodies for detection of actin as a loading control. Mr, molecular weight markers.
D. The effect of *LdCOF* disruption on *in vitro* growth of *L. donovani* promastigotes. The *LdCOF*$^{+/+}$ (diamonds), *LdCOF*$^{+/-}$ (circles) and *LdCOF*$^{-/-}$ (squares) cells were grown in DMEM containing 10% FCS without antibiotics. Initial cell density was about 1×10^6 cells ml^{-1}. Growth analysis was done under shaking at 50 r.p.m. The values shown are means of three independent experiments ± standard deviation. Significant reduction in growth was seen in both *LdCOF*$^{+/-}$ and *LdCOF*$^{-/-}$ cells, compared with *LdCOF*$^{+/+}$ cells.

the *LdCOF*$^{+/+}$ cells. Also the axonemal attachment fibres were absent, and in about 53% sections, membrane-bound vesicles appeared to accumulate in the flagellum (Fig. 8B). Out of the 53%, about 80% sections showed vesicles at the flagellar tip and the remaining 20% sections showed the presence of vesicles along the entire length of the flagellum. In addition, about 17% of the flagellar sections showed the presence of electron-dense intraflagellar transport (IFT)-like particles. However, in all the sections that were analysed the classical 9 + 2 arrangement of the microtubules in the axoneme was largely conserved. No abnormalities were seen in the Golgi apparatus, kinetoplast and nucleus of the mutant cells.

The absence of PFR in the *LdCOF*$^{+/-}$ and *LdCOF*$^{-/-}$ cells was further confirmed by immunofluorescence microscopy and immunoblotting using mAb2E10 antibody (Ismach *et al.*, 1989), which detects PFR1 and PFR2 in *LdCOF*$^{+/+}$ cells. The flagellum of the *LdCOF*$^{+/+}$ cells was intensely stained by mAb2E10, whereas no such staining was observed in the mutant cells, indicating the absence of PFR1 and PFR2 in the flagellum of these cells (Fig. 8C). These results were further corroborated by the complete absence of these proteins in whole-cell lysates of *LdCOF*$^{+/-}$ and *LdCOF*$^{-/-}$ cells (Fig. 8D).

Episomal complementation of LdCof restored flagellar phenotype and motility

To unequivocally establish that the observed abnormalities are directly related to the depletion of LdCof in *Leishmania*, we transfected the *LdCOF*$^{-/-}$ cells with plasmid p6.5MCS containing the full-length *LdCOF* gene tagged with GFP at its N-terminus (*p6.5GFP–LdCOF*). The *LdCOF*$^{-/-}$ mutants transfected with p6.5MCS vector alone were used as the transfection control. The transfected cells were selected on DMEM agar plates containing 10 μg ml^{-1} tunicamycin. The resulting selected colonies

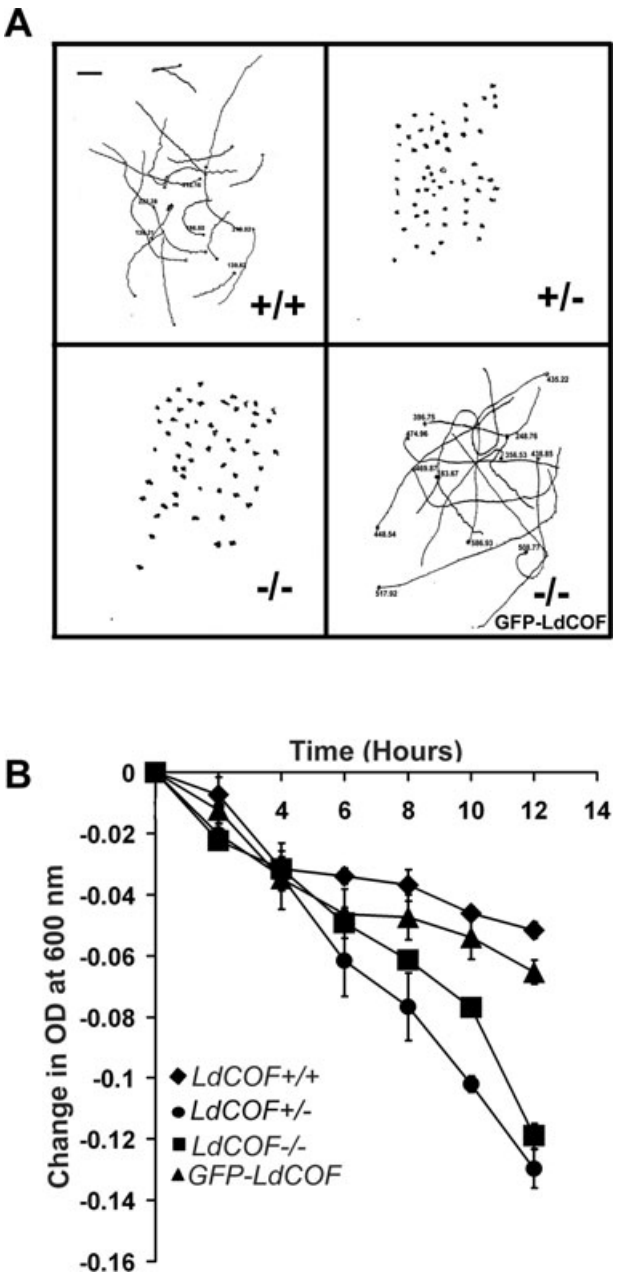

Fig. 6. Motility analysis of *LdCOF* mutants by time lapse microscopy and sedimentation assay.
A. Traces of paths of live, individual cells in the movies indicate that *LdCOF*$^{+/-}$ and *LdCOF*$^{-/-}$ cells are completely immotile. However, upon episomal complementation of *LdCOF*$^{-/-}$ cells, the motility is restored back to normal. Origin of the path is indicated by solid dots. Bar, 50 μm. Total path lengths were measured using 'Leica Qwin' software (Leica, Germany) and mentioned along the traces.
B. Analysis of cell motility by sedimentation assay. *LdCOF*$^{+/+}$ cells (diamonds) and episomally complemented null mutants (triangles) did not settle down despite leaving them under standing conditions for 12 h, whereas most of *LdCOF*$^{+/-}$ (circles) and *LdCOF*$^{-/-}$ (squares) cells settled at the bottom of the cuvette within this time period. Values shown are means of three independent experiments ± standard deviation.

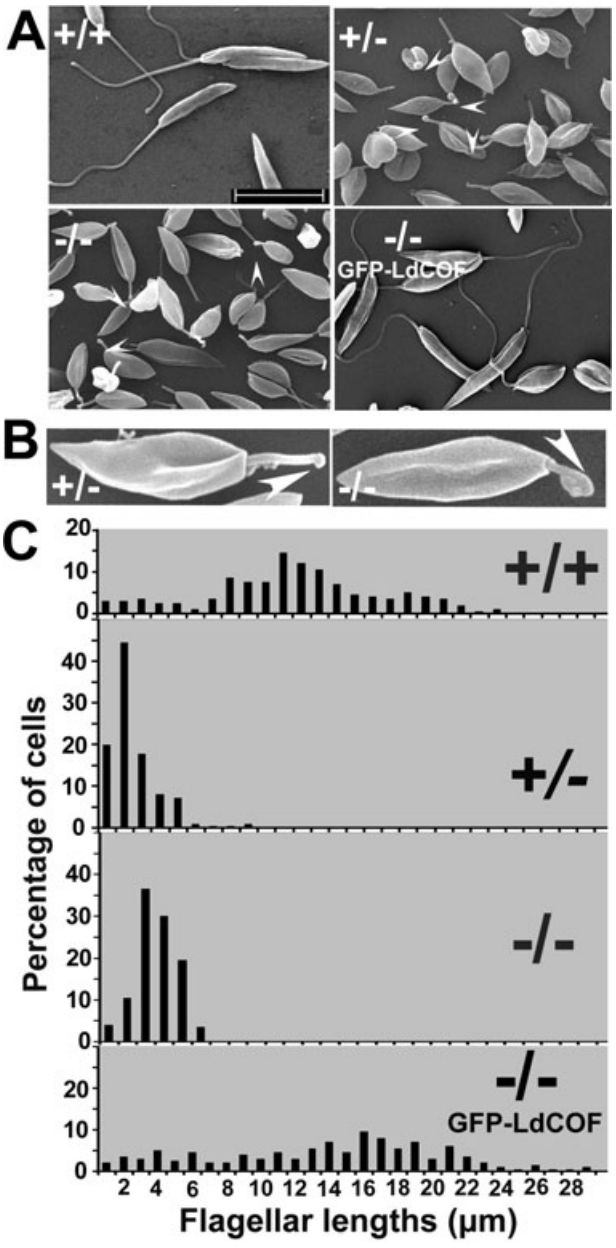

Fig. 7. A. Analysis of cell shape and flagellar length by scanning electron microscopy showing typical morphology of *LdCOF*$^{+/+}$ cells and short and stumpy cell body and reduced flagellar length of *LdCOF* mutants. Episomal complementation of *LdCOF*$^{-/-}$ cells resulted in regain of the wild-type morphology and flagellar length. Bar, 10 μm. Arrow heads indicate the 'blob-like' structures seen at the tip and at various positions on the flagella of mutant cells.
B. Magnified images of *LdCOF*$^{+/-}$ and *LdCOF*$^{-/-}$ cells showing 'blob-like' structures.
C. Histogram of flagellar lengths of *LdCOF*$^{+/+}$, *LdCOF*$^{+/-}$, *LdCOF*$^{-/-}$ and GFP–LdCof-complemented *LdCOF*$^{-/-}$ cells. More than 200 cells were analysed from each cell line.

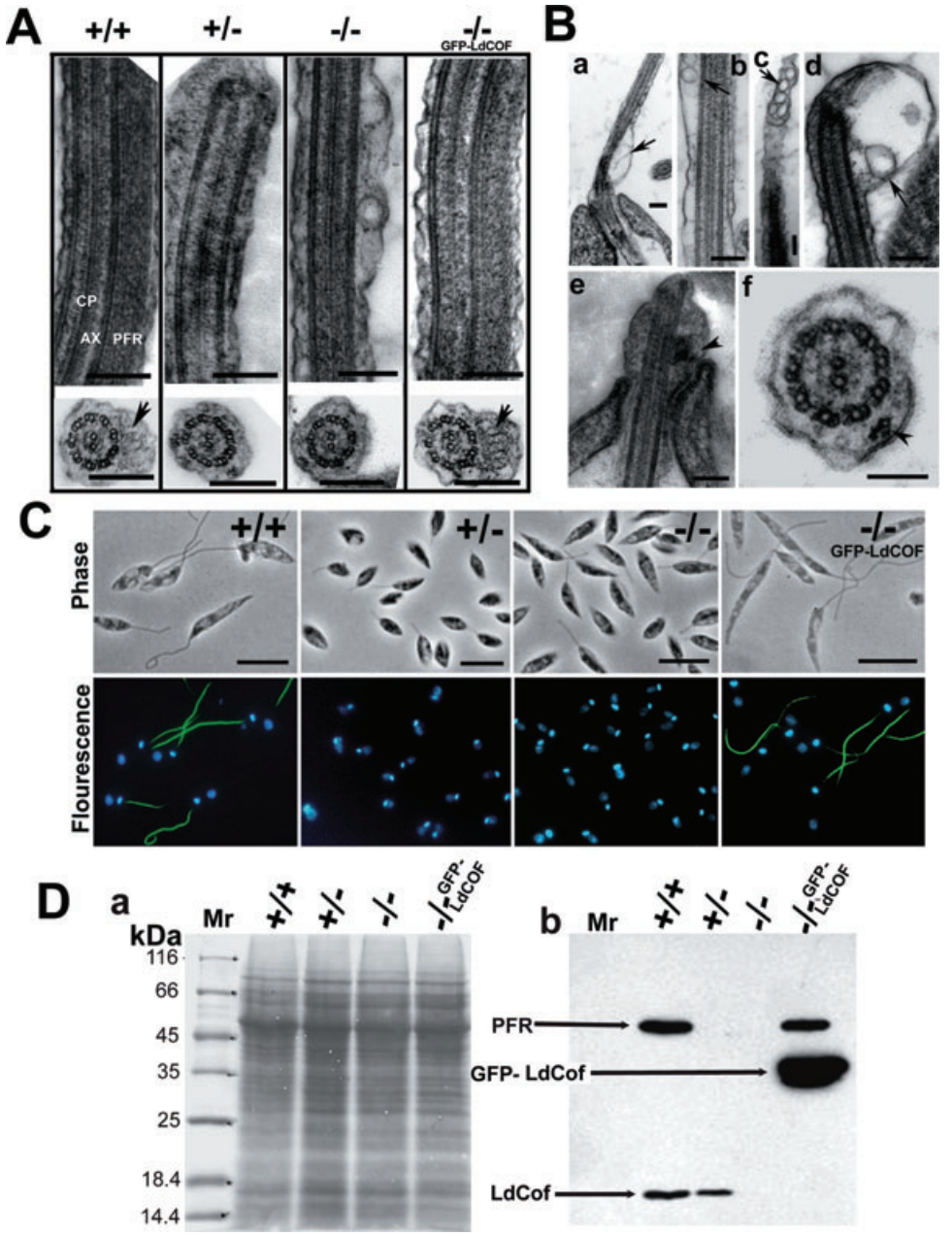

Fig. 8. A. Transmission electron micrographs of thin sections of flagellum from chemically fixed whole cells showing the absence of PFR in *LdCOF*$^{+/-}$ and *LdCOF*$^{-/-}$ cells and its restoration upon episomal complementation. Longitudinal sections of the flagellum showing the axoneme (AX) with the central pair microtubules (CP) and PFR confined between the axoneme and the flagellar membrane in wild type and GFP–LdCof-complemented cells. Bar, 200 nm. Cross sections of the flagellum showing the PFR in *LdCOF*$^{+/+}$ (marked by arrow) and GFP–LdCof-complemented cells, and complete absence of this structure in the cross sections of *LdCOF*$^{+/-}$ and *LdCOF*$^{-/-}$ cells. Bar, 200 nm.
B. Accumulation of membrane-bound vesicles in the flagella of mutant cells. (a–d) Longitudinal sections of chemically fixed whole cells of *LdCOF*$^{-/-}$ mutants showing accumulation of membrane-bound vesicles at the base (a), along the length (b and c) and tip (d) of the mutant flagellum. Arrows indicate the membrane-bound vesicles. Longitudinal section (e) and cross section (f) of chemically fixed whole cells of *LdCOF*$^{-/-}$ mutant showing IFT-like particles along the length of the flagellum. Arrow heads indicate IFT-like particles. Bar, for (a–e) 200 nm and for (f) 100 nm.
C. Loss of PFR assembly in *LdCOF*$^{+/-}$ and *LdCOF*$^{-/-}$ mutants and its restoration in episomally complemented cells. Whole cells were processed for immunofluorescence analysis as described in *Experimental procedures*. PFR1 and PFR2 proteins were stained with mAb2E10 antibodies. Nuclear and kinetoplast DNA stained with DAPI. Intense staining of flagella was observed in *LdCOF*$^{+/+}$ and episomally complemented null mutants. However, no staining of flagellum was seen in *LdCOF*$^{+/-}$ and *LdCOF*$^{-/-}$ mutants. Phase contrast images show restoration of wild-type cell morphology in episomally complemented null mutants. Bar, 5 μm.
D. Western blot analysis of PFR proteins in total cell lysates (10 μg protein per lane). (a) Coomassie blue-stained 12% SDS-PAGE. Mr, molecular weight markers. (b) Western blot of (a) using mAb2E10 antibodies and rabbit anti-rLdCof antibodies.

were proliferated in DMEM liquid medium containing 10 μg ml^{-1} tunicamycin. The *p6.5GFP–LdCOF*-transfected null mutants abundantly expressed the GFP–LdCof fusion protein, as confirmed by both Western blot analysis (Fig. 8D) and GFP fluorescence. These episomally complemented *LdCOF*$^{-/-}$ cells regained wild-type cell morphology (Fig. 7A), flagellar length [13.92 ± 6.02 μm (n = 208); Fig. 7C], motility (Fig. 6A and B; also see Movie S3) and flagellar beat, whereas the control cells were still stumpy and immotile with short flagellum. Furthermore, transmission and immunofluorescence microscopic analysis of these cells revealed that the PFR structure had been restored and all other abnormalities that were observed in flagellar structure in the null mutants disappeared (Fig. 8A, C and D), confirming that the observed defects in the flagellum assembly and motility in the heterozygous and the homozygous mutants were primarily due to depletion of ADF/cofilin.

LdCof depletion affects the intracellular distributions of actin and LdCof in Leishmania

ADF/cofilins localize to cellular regions that have high actin dynamics, such as the leading edge of pseudopodium, and have therefore been implicated in cellular motility (Theriot, 1997; Ghosh *et al*., 2004). LdCof was concentrated in the anterior region including the flagellar base of wild-type cells (Fig. 1C). In order to understand the functional significance of this differential LdCof localization, we analysed the intracellular distribution of LdCof as well as actin in the *LdCOF*$^{+/-}$, *LdCOF*$^{-/-}$ and GFP–LdCof-complemented *LdCOF*$^{-/-}$ cells (Fig. 9). LdCof distribution in *LdCOF*$^{+/+}$ cells was polarized towards the anterior region including the flagellar base where it colocalized with patch-like structures of actin. However, no such distribution of LdCof was observed in *LdCOF*$^{+/-}$ cells. This apart, in contrast to the *LdCOF*$^{+/+}$ cells where actin was diffusely distributed throughout the flagellum, this protein was completely absent in the short and paralysed flagellum of *LdCOF*$^{-/-}$ cells, and a lot of it accumulated in the flagellum of *LdCOF*$^{+/-}$ cells. Furthermore, almost all *LdCOF*$^{-/-}$ cells contained actin in its filamentous form, whereas it was predominantly present in the form of granules and patches in *LdCOF*$^{+/+}$ cells. However, normal actin and LdCof distributions were restored after episomal complementation. These results clearly suggest that LdCof-driven actin dynamics plays a critical role in assembly of the *Leishmania* flagellum.

Discussion

This study shows that *Leishmania* contains an ADF/cofilin homologue that binds the filamentous as well as monomeric forms of *Leishmania* actin and depolymerizes the filamentous form into monomers. It further shows that *Leishmania* cells that are deficient in this protein are completely immotile, have reduced flagellar length and cell growth, and have short and stumpy cell body, as compared with the wild-type cells. Also, flagellar beat is severely impaired and the PFR structure is not made. In addition, vesicle-like structures appear throughout the length including tip of the flagellum. However, all these abnormalities are removed by episomal complementation. Together, these results demonstrate that LdCof is essentially required in assembly and motility of the *Leishmania* flagellum.

It is intriguing that phenotypic characters of heterozygous *LdCOF* mutants are similar to those of homozygous mutants despite the differences in their LdCof contents as well as intracellular actin distributions. As LdCof in the wild-type cells is concentrated in the anterior region in association with actin and such a polarized LdCof distribution is absent in a majority of the heterozygous mutants (in > 90% cells) and several earlier studies have shown accumulation of various flagellar proteins at the flagellar base prior to their targeting to the flagellum (Bloodgood, 2000), we speculate that LdCof-driven actin dynamics is perhaps required in intracellular trafficking (Reisler, 1993) of the flagellar proteins from the cytoplasm to the flagellar base. Failure of cells to traffic these proteins to the flagellar base may then account for phenotypic similarities between the heterozygous and homozygous mutants. Further, as actin is present throughout the cell including the flagellum where LdCof is also available, we speculate that both these proteins may be required in assembly of the flagellum, especially the PFR.

Flagellar assembly is an intricate process that co-ordinates the transportation and organization of proteins into the flagellum. Some protozoans also accommodate synthesis of a novel cytoskeletal structure, called the PFR (Bastin *et al*., 1996). PFR is present in kinetoplastids, euglenoids and dinoflagellates, and is essential for *Leishmania* and *Trypanosoma* cell motility (Santrich *et al*., 1997; Bastin *et al*., 1998). The absence of PFR structure in *LdCOF*$^{-/-}$ cells and its subsequent reappearance upon episomal complementation suggest that LdCof is essentially required for assembly of the PFR structure in *Leishmania.* The absence of PFR proteins in both the heterozygous and homozygous mutants could mainly be due to their rapid degradation in the cytoplasm, which has also been suggested by the earlier studies (Maga *et al*., 1999; Adhiambo *et al*., 2005). It should be noted that the observed defects in the flagellar motility and beat are not merely due to absence of the PFR, as the PFR1, PFR2 and PFR1 and two deletion mutants at least partially retain their motility, and have an altered waveform of flagellar beat (Maga *et al*., 1999). This suggests that besides PFR1 and

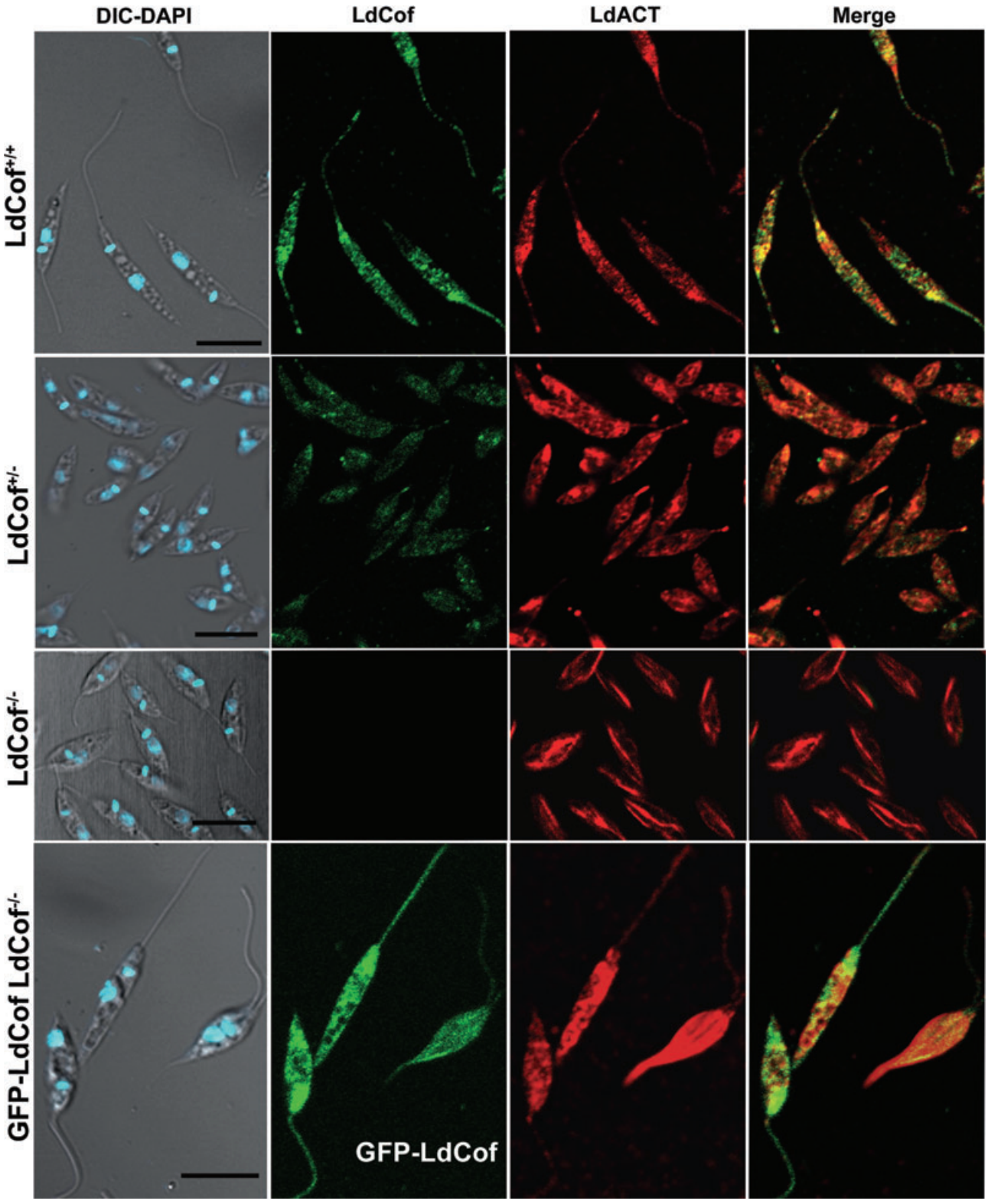

Fig. 9. LdCof depletion results in altered LdCof and actin distributions in LdCof mutant cells. Intracellular distribution of LdCof is polarized towards the anterior region in *LdCOF*$^{+/+}$ cells, whereas this protein is almost uniformly distributed in *LdCOF*$^{+/-}$ cells. Further, in contrast to *LdCOF*$^{+/+}$ cells, where actin is localized throughout the flagellum, this protein is completely absent in the flagellum of *LdCOF*$^{-/-}$ cells, and a lot of it accumulated in the flagellum of *LdCOF*$^{+/-}$ cells. However, normal LdCof and actin distributions were restored after episomal complementation. In each case at least 1000 cells were assessed for intracellular distributions of LdCof and actin. Bar, 5 μm.

PFR2 proteins, LdCof deletion might have also affected the recruitment of various other proteins that are critical in maintaining normal flagellar beat and motility.

The flagellum is a dynamic organelle and its length varies with the stage and differentiation of *Leishmania* parasites. As flagellar assembly requires continuous recycling of several components, flagellar length control must rely upon regulation of IFT (Rosenbaum and Witman, 2002; Rosenbaum, 2003). As flagellar length of the PFR1, PFR2 and PFR1 and two knockouts in *Leishmania* have been reported to be similar to that of wild-type cells with normal axonemes (Santrich *et al*., 1997; Maga *et al*., 1999), we infer that the short flagellum phenotype observed here is a direct consequence of LdCof deletion and not only due to the lack of PFR. Furthermore, the *LdCOF*$^{-/-}$ cells appear, to some extent, similar to the flagellar phenotype of *Leishmania*, *Chlamydomonas* and *Caenorhabditis elegans* where dynein-2 is disrupted. In *Leishmania*, disruption of dynein-2 resulted in short, non-emergent flagella with disorganized axonemes (Adhiambo *et al*., 2005). In *Chlamydomonas*, disruption of this protein resulted in bulbous and stumpy (1–2 μm length), non-motile flagella filled with aberrant microtubules, IFT raft-like particles and other amorphously stained material (Pazour *et al*., 1999; Porter *et al*., 1999). Similarly, mutation of dynein-2 in *C. elegans* resulted in swollen, shorter sensory cilia filled with electron-dense material (Signor *et al*., 1999; Wicks *et al*., 2000). Further, a novel microtubule-depolymerizing kinesin has recently been shown to regulate flagellar length in *Leishmania* (Blaineau *et al*., 2007). Taken together, these studies suggest that proper flagellar assembly requires the transport of the flagellar components from the cytoplasm to the tips of the flagellar microtubules where they are added to the microtubule ends. Earlier, it has been reported that Kinesin II and cytoplasmic dynein (DHC1b) play a key role in anterograde (base to tip) and retrograde (tip to base) IFT respectively (Kozminski *et al*., 1993; Pazour *et al*., 1998; 1999). Defects in IFT have been shown to result in accumulation of electron-dense particles in the flagellum in *Chlamydomonas* and *Trypanosoma* (Porter *et al*., 1999). However, unlike these organisms, disturbance in IFT by knocking out dynein did not result in accumulation of electron-dense material in *Leishmania* (Adhiambo *et al*., 2005). Unlike the dynein knockouts, a significant fraction (~17%) of flagellar sections of *LdCOF*$^{+/-}$ and *LdCOF*$^{-/-}$ cells showed accumulation of electron-dense material. These observations suggest that LdCof-driven actin dynamics may also be required in IFT in *Leishmania*. This finds strong support from an earlier study that suggested that the movement of extra-axonemal proteins, such as PFR proteins, is also through IFT (Bastin *et al*., 1999).

Deletion of LmxMKK (MAP kinase) in *L. mexicana* has been shown to result in reduction of flagellar length and axonemal defects (Wiese *et al*., 2003). Also a targeted deletion of another MAP kinase homologue in the same organism (LmxMPK3) is known to result in flagellar length defects, loss of PFR assembly, accumulation of membrane vesicles and fragments at the flagellar tip and pocket respectively. These two kinases have been hypothesized to be the components of a possible MAP kinase cascade for flagellar morphogenesis or may be involved in IFT of proteins (Erdmann *et al*., 2006). As ADF/cofilin is reversibly activated by phosphatases and inhibited by LIM kinases (Ono, 2007), which are absent in the *Leishmania* genome (Berriman *et al*., 2005), we suggest that LdCof could be a downstream effector of the MAP kinase pathway as one of the above kinases may serve the function of LIM kinase in these organisms.

Finally, around 331 proteins have been described to constitute the flagellar proteome (Broadhead *et al*., 2006). However, the mechanisms of their targeting into the flagellum and cilia have not yet been fully elucidated (Fridberg *et al*., 2007). The results presented here, for the first time, demonstrate that an actin dynamics-regulating protein, LdCof, in *Leishmania* plays a critical role in flagellar assembly and motility. However, further studies are required to precisely understand the mechanisms that underlie in LdCof-based regulation of the intraflagellar transport.

Experimental procedures

Cloning of Leishmania *ADF/cofilin (LdCof) and human cofilin (HCof)*

Gene-specific primers were designed on the basis of *Leishmania major* putative cofilin gene sequence available from the gene bank (accession No. XM_842616). Cofilin gene (429 base pairs) from *Leishmania donovani* was amplified by polymerase chain reaction (PCR) using the *L. donovani* genomic DNA as the template and forward (P1) and reverse (P2) primers. To amplify human cofilin (*HCof*) gene, total RNA was isolated from cultured HeLa cells and used as the template for the first-strand cDNA synthesis (Qiagen). *HCof* gene was amplified using sequence-specific primers (forward P3 and reverse P4). PCR-amplified products from *L. donovani* (cofilin gene) and human (cofilin gene) were cloned at NcoI and NotI sites in frame with hexa-histidine tag of the pET21d overexpression vector. Cloned sequences of both the *Leishmania* cofilin (*LdCof*) and human cofilin (*HCof*) genes were sequenced by dideoxy chain termination method. *LdCof* gene sequence thus obtained was submitted to EMBL gene bank (Accession No. DQ010161) whereas *HCof* gene sequence matched 100% with human cofilin gene (Accession No. X95404.1).

Proteins

Both *LdCof* and *HCof* were expressed with a hexa-histidine tag at their C-terminus (hereafter referred as rLdCof and

rHCof respectively) in BL21 (DE3) Rossetta strain (Novagen). Transformed *Escherichia coli* cells with the expression constructs were grown to an OD_{600} of 0.5 and expression was induced with 0.04 mM isopropyl β-D-thiogalactoside. *LdCof*-transformed *E. coli* were grown and induced at 20°C and *HCof*-transformed *E. coli* were grown and induced at 37°C. Cells were harvested after 5 h of growth and suspended in 50 mM sodium phosphate, pH 8.0, 300 mM NaCl containing 0.2 mM phenylmethylsulfonyl fluoride (Sigma) and lysed by sonication. Lysates were clarified by centrifugation at 30 000 *g* at 4°C, adjusted to 20 mM imidazole and applied to Ni-NTA Sepharose Fast Flow columns (Qiagen) equilibrated with 50 mM sodium phosphate, pH 8.0, 300 mM NaCl and 20 mM imidazole. Columns were washed thoroughly with 50 mM sodium phosphate (pH 8.0), 500 mM NaCl containing 30 mM imidazole and eluted by increasing the imidazole concentration to 50 mM or 200 mM for *rLdCof* or *rHCof* respectively. Eluates were dialysed into 5 mM HEPES (pH 7.4), 2 mM dithiothreitol and 1 mM NaN_3. Purity of proteins was analysed by SDS-PAGE.

Leishmania actin was purified from cultured insect cells (SF9) infected with recombinant baculovirus harbouring *Leishmania* actin gene, essentially as described earlier (Kapoor *et al*., 2008). Rabbit skeletal muscle actin was purified from rabbit muscle acetone powder as described by Pardee and Spudich (1982) and stored in lyophilized form at –80°C after addition of sucrose (2 mg mg^{-1} protein). G-actin was subjected to size exclusion chromatography each time after thawing a new frozen vial, and only the peak fractions of monomeric actin were used in the experiments. To prepare ADP.actin monomers, excess ATP was removed by repeated washing through 30 kDa cut-off Centricon (Millipore, USA) using G-buffer (5 mM Tris-Cl pH 8.0, 0.2 mM $CaCl_2$, 0.5 mM DTT and 0.2 mM NaN_3) and then a mixture of 10 μM actin and 0.5 mM ADP was incubated at 4°C overnight.

Biotin labelling of actin was done as described by Okabe and Hirokawa (1989). Biotin incorporation was confirmed by Western blot analyses of labelled actin using HRP-conjugated antibiotin antibodies (New England Biolabs, USA).

F-Actin binding and depolymerization

F-actin sedimentation assay of rabbit muscle actin (actin) and *Leishmania* actin (LdACT) was done as described by Ono and Benian (1998) and Kapoor *et al*. (2008), respectively, in presence of varied concentrations of *rLdCof* and *rHCof*. The supernatants and the pellets were adjusted to the same volume and analysed by 12% SDS-PAGE. After staining with Coomassie Brilliant Blue-R250, gels were scanned and band densities were quantified using ImageMaster software (Amersham Pharmacia).

For the pH-dependent experiments, F-actin was incubated for 1 h at room temperature with *rLdCof* or *rHCof* in the buffers containing 100 mM KCl, 2 mM $MgCl_2$, 1 mM dithiothreitol, 2 mM ATP, 0.2 mM $CaCl_2$, 0.5 mM NaN_3, together with 20 mM 2-(N-morpholino)ethanesulfonic acid (pH 6.0 and 6.5) or 20 mM HEPES-NaOH (pH 7.5) or 20 mM Tris-HCl (pH 8.5 and 9.0). The mixtures were centrifuged at 140 000 *g* for 20 min. The supernatant and pellet fractions were analysed by 12% SDS-PAGE.

Actin depletion pull-down assay

Actin monomer binding with rLdCof was assessed by actin depletion pull-down assay as described by Mattila *et al*. (2004). Monomers of ADP.actin and ATP.actin (5 μM each) were incubated separately with varying concentrations of rLdCof for 1 h at room temperature and then Ni-NTA superflow beads (Qiagen, USA) were added to the reaction mixture. It was centrifuged briefly to settle down any bead-bound proteins and the supernatants were collected. After thorough washing of the beads with the G-buffer containing 0.5 mM ADP or ATP, bead-bound proteins were collected after releasing them in 100 mM EDTA in G-buffer. Bead-bound and free actin were analysed by 12% SDS-PAGE.

Binding of rLdCof with LdACT was assessed by using lysates of LdCof null (*LdCOF*$^{-/-}$) mutants. The cells were lysed by sonicating briefly in G-buffer containing 0.5 mM ADP and clear supernatant was collected after centrifugation at 100 000 *g* for 1 h at 4°C. The lysate was pre-treated with Ni-NTA beads and then incubated with varying concentrations of rLdCof for 1 h on ice. Supernatants and bead-bound proteins were separated as above and LdACT in these fractions was detected by Western blotting using anti-LdACT antibodies. Band intensities of Coomassie-stained gels or Western blots were quantified using ImageMaster software (Amersham Pharmacia).

Nucleotide exchange and severing assays

Nucleotide exchange in the steady-state F-actin solutions labelled with 1,N6-ethenoadenosine 5′-triphosphate (ε-ATP; Molecular Probes, USA) was performed essentially as described by Carlier *et al*. (1997). The filament-severing activity of cofilins was microscopically observed as described by Ono *et al*. (2004). The filaments lengths were calculated using 'Leica QWin' software (Leica, Germany).

Flanking sequences and gene-targeting constructs

The 5′ and 3′ flanking sequences of *LdCOF* in *L. donovani* were determined by using standard procedures. Primers were designed based on the available *L. infantum* genomic data to amplify approximately 1 kb regions of the 5′ and 3′ flanking sequences. For the amplification of 5′ flanking region three forward primers (P5, P6, P7) from the intergenic region and one reverse primer (P8) from the *LdCOF* gene were designed such that the amplicons generated will be approximately 1 kb each and can give amplification using internal primers for the confirmation of specific amplification of the 5′ flank sequence of *LdCOF* gene. Similarly, one forward primer (P9) from *LdCOF* gene and two reverse primers (P10, P11) from the 3′ intergenic region were designed for the specific amplification of the 3′ flank region. The 5′ and 3′ flanking regions were amplified using *L. donovani* genomic DNA as the template and the amplicons were cloned into InsT/A clone (MBI Fermentas) and sequenced by dideoxy method for designing *LdCOF* gene deletion constructs. Sequences thus obtained were submitted to EMBL.

The 5′ and 3′ flank regions of *LdCOF* gene were amplified from *L. donovani* genomic DNA template using forward

(P12), reverse (P13) and forward (P18), reverse (P19) primers respectively. The amplified 5′ and 3′ flanking regions were cloned into pGEMT Easy (Promega) and InsT/A vectors respectively, and forward-oriented clones were selected (hereafter referred as 5′*FLK*/pGEMT and 3′*FLK*/InsT/A). Hygromycin phosphotransferase (*HYG*) and neomycin phosphotransferase (*NEO*) genes were amplified from pCDNA3 and pXG-GFP vectors (kind gift from Dr. S.M. Beverley) respectively, and their respective open reading frames tagged with M-sequence through primers at their 5′ ends. These resistance markers were amplified by PCR using forward (P14) and reverse (P15), and forward (P16) and reverse (P17) primers respectively, and cloned into InsT/AClone vector separately and forward-oriented clones were selected. *HYG* and *NEO* gene cassettes were cloned separately into 5′FLK/pGEMT construct by digesting at HindIII and XhoI sites, resulting in 5′*FLK*/*HYG* and 5′*FLK*/*NEO* constructs. 5′*FLK/NEO* fragment from 5′*FLK/NEO*/InsT/A was digested at EcoRI and XhoI sites and cloned into 3′*FLK*/InsT/A, resulting in the final gene deletion cassette containing 5′ and 3′ flank regions flanking the *NEO* cassette (hereafter referred as 5/3 *NEO*). Similarly, 3′ flank construct from 3′*FLK*/InsT/A was digested at XhoI and SalI sites and cloned into 5′*FLK/HYG*/pGEMT Easy, resulting in the gene deletion construct containing 5′ and 3′ flank regions flanking the hygromycin cassette (hereafter referred as 5/3 *HYG*).

For episomal complementation, *LdCOF* gene was first cloned into pXG-GFP+2/vector at BglII site that added GFP at its N-terminus, and was subsequently subcloned into p6.5MCS vector (kind gift from Dr. K.P. Chang) as *GFP–LdCOF* fusion product using forward (P20) and reverse (P21) primers.

Please see Table S1 for primer sequences.

Leishmania *cultures and genetic manipulations*

Leishmania donovani cells were maintained in high-glucose DMEM supplemented with 10% heat-inactivated fetal bovine serum and 40 mg l^{-1} gentamicin at 25°C. Transfection of *Leishmania* promastigotes was achieved by electroporation as described (Nayak *et al.*, 2005). The *LdCOF* single- and double-allele deletion mutants (*LdCOF*$^{+/-}$ and *LdCOF*$^{-/-}$) of *L. donovani* were selected against 50 μg ml^{-1} G-418 and/or 50 μg ml^{-1} hygromycin. Episomally complemented *LdCOF* null cells (*GFP–LdCOF*) were maintained in high-glucose DMEM containing 50 μg ml^{-1} each of G-418 and hygromycin as well as 10 μg ml^{-1} tunicamycin. For Southern hybridizations, genomic DNA (10 μg) from *LdCOF*$^{+/+}$, *LdCOF*$^{+/-}$ and *LdCOF*$^{-/-}$ cells was digested with XhoI enzyme, resolved on 0.8% agarose gel and transferred onto nylon membrane (Hybond N+, Amersham Pharmacia). Hybridization was carried out by using DIG-labelled probe prepared against *LdCOF*, *NEO* and *HYG* gene cassettes. Signals were detected using chemiluminescence substrate on an X-ray film.

Antibodies, Western blotting and immunofluorescence

The FPLC-purified rLdCof was emulsified in Freund's complete adjuvant by passing forcibly through a 22 gauge needle and the emulsion was immediately injected subcutaneously into rabbits and mice. Animals were bled on 10th day after the booster dose with rLdCof emulsified in Freund's incomplete adjuvant. Polyclonal antibodies were affinity-purified by using purified rLdCof coupled to CNBr-activated Sepharose beads (Amersham Pharmacia Biotech). Antibodies against *Leishmania* actin were prepared as described (Sahasrabuddhe *et al.*, 2004). Anti-α,β-tubulin antibodies were procured from Sigma, USA and anti-PFR antibodies (mAb2E10) were a kind gift from Dr. Diane Mc Mahon Pratt. Lysates of *LdCOF*$^{+/+}$, *LdCOF*$^{+/-}$ and *LdCOF*$^{-/-}$ cells were prepared by re-suspending and boiling the cell pellets for 5 min in 1× SDS-sample buffer. Samples were resolved on SDS-PAGE (12% resolving) and electro-blotted onto nitrocellulose membrane (Pall, USA). LdCof, actin and PFR were detected using anti-LdCof antibodies, anti-*Leishmania* actin antibodies and monoclonal mAb2E10 antibodies respectively. Blots were developed by using Chemiluminiscence substrate (Millipore) and signals were collected on X-ray films. Immunofluorescence microscopy was performed as described (Nayak *et al.*, 2005) and LdCof, *Leishmania* actin and PFR proteins were probed with their respective antibodies. Images were captured on ZEISS LSM510 META Confocal Microscope using 63 × 1.4 NA (oil) Plan Apochromate lens.

Scanning and transmission electron microscopy

For scanning electron microscopy, cells were fixed with 4% paraformaldehyde and 1% glutaraldehyde in 0.1 M sodium cacodylate buffer (pH 7.4) and cell suspensions were placed on poly-L-lysine (0.1%)-coated coverslips and allowed to adhere for 45 min in a humid chamber. Cells were postfixed in 1% osmium tetroxide for 1 h at room temperature and were dehydrated in an ascending series of ethanol, critical point dried and coated with Au-Pd (80:20) using a sputter coater (Polaron E5000). Samples were examined in a Philips XL30 ESEM at an accelerating voltage of 30 kV. About 200 cells were analysed for each sample. For transmission electron microscopy, cells were fixed with 1% glutaraldehyde in DMEM without FCS for 15 min at room temperature and then with 1% gluteraldehyde in 0.1 M sodium cacodylate buffer (pH 7.4) for 1 h. After repeated washes with buffer, the cells were postfixed with 1% OsO_4 in sodium cacodylate buffer at room temperature for 2 h and encapsulated in 2% low-melting agarose (Sigma, USA). Samples were stained *en bloc* with 1% aqueous uranyl acetate, dehydrated in an ascending series of ethanol, embedded in Epon-Araldite plastic mixture and polymerized at 60°C for 24 h. Ultra thin sections (50–70 nm) were picked up onto 200 mesh copper grids and were doubly stained with uranyl acetate and lead citrate. Sections were analysed under a FEI Tecnai-12 Twin Transmission Electron Microscope equipped with a SIS Mega View II CCD camera at 80 kV (FEI Company, USA).

Motility assessment by sedimentation and time lapse microscopy

Motility assessment by sedimentation assay was performed by monitoring optical density at 600 nm (OD_{600}) at different time intervals. The value obtained by subtracting the OD_{600} value of the re-suspended controls from the OD_{600} value of

the settled cells was plotted. Motility was also monitored by time lapse microscopy at eight frames per second on ZEISS LSM510 META. Paths of individual cells displayed on the time lapse movie were traced manually and path lengths were measured using 'Leica QWin' software (Leica, Germany). Flagellar beat function was monitored again by time lapse microscopy as above but the cells were attached to 0.001% poly-L-lysine-coated glass coverslips in order to partly immobilize the cell body movements.

Acknowledgements

This work was partially supported from the research grant awarded to C.M.G. by the Department of Biotechnology, Government of India, New Delhi (India) under the Distinguished Biotechnologist Award Scheme. T.V.S.T. is a recipient of Research Fellowships from the Council of Scientific and Industrial Research, Rafi Marg, New Delhi (India). We are Grateful to Dr. A.N. Ghosh (NICED, Kolkata) for his help in electron microscopy. This is a Communication No. 7522 from CDRI, Lucknow (India).

References

Absalon, S., Blisnick, T., Kohl, L., Toutirais, G., Doré, G., Julkowska, D., *et al.* (2008) Intraflagellar transport and functional analysis of genes required for flagellum formation in trypanosomes. *Mol Biol Cell* **3:** 929–944.

Adhiambo, C., James, D.F., David, J.A., and LeBowitz, J.H. (2005) The two cytoplasmic dynein-2 isoforms in *Leishmania mexicana* perform separate functions. *Mol Biochem Parasitol* **143:** 216–225.

Afzelius, B.A. (2004) Cilia-related diseases. *J Pathol* **204:** 470–477.

Andrianantoandro, E., and Pollard, T.D. (2006) Mechanism of actin filament turnover by severing and nucleation at different concentrations of ADF/cofilin. *Mol Cell* **6:** 13–23.

Bastin, P., Matthews, K.R., and Gull, K. (1996) The paraflagellar rod of Kinetoplastida: solved and unsolved questions. *Parasitol Today* **12:** 302–307.

Bastin, P., Sherwin, T., and Gull, K. (1998) Paraflagellar rod is vital for *Trypanosome* motility [letter]. *Nature* **391:** 548.

Bastin, P., Pullen, T.J., Sherwin, T., and Gull, K. (1999) Protein transport and flagellum assembly dynamics revealed by analysis of the paralysed trypanosome mutant snl-1. *J Cell Sci* **112:** 3769–3777.

Berriman, M., Ghedin, E., Hertz-Fowler, C., Blondin, G., Renauld, H., Bartholomeu, D.C., *et al.* (2005) The genome of African trypanosome *Trypanosoma brucei*. *Science* **309:** 416–422.

Blaineau, C., Tessier, M., Dubessay, P., Tasse, L., Crobu, L., Pagès, M., and Bastien, P. (2007) A novel microtubule-depolymerizing kinesin involved in length control of a eukaryotic flagellum. *Curr Biol* **17:** 778–782.

Blondin, L., Spauntzi, V., Maciver, S.K., Lagarrigue, E., Benyamin, Y., and Roustan, C. (2002) A structural basis for pH-dependence of cofilin F-actin interactions. *Eur J Biochem* **269:** 4194–4201.

Bloodgood, R.A. (2000) Protein targeting to flagella of trypanosomatid protozoa. *Cell Biol Int* **24:** 857–862.

Broadhead, R., Dawe, H.R., Farr, H., Griffiths, S., Hart, S.R., Portman, N., *et al.* (2006) Flagellar motility is required for the viability of the bloodstream trypanosome. *Nature* **440:** 224–227.

Carlier, M.F., Laurent, V., Santolini, J., Melki, R., Didry, D., Xia, G.X., *et al.* (1997) Actin depolymerizing factor (ADF/cofilin) enhances the rate of filament turnover: implications in actin based motility. *J Cell Biol* **136:** 1307–1322.

Dos Remedios, C.G., Chhabra, D., Kekic, M., Dedova, I.V., Tsubakihara, M., Berry, D.A., and Nosworthy, N.J. (2003) Actin binding proteins: regulation of cytoskeletal microfilaments. *Physiol Rev* **83:** 433–473.

Erdmann, M., Scholz, A., Melzer, I.M., Schmetz, C., and Wiese, M. (2006) Interacting protein kinases involved in the regulation of flagellar length. *Mol Biol Cell* **17:** 2035–2045.

Fridberg, A., Buchanan, K.T., and Engman, D.M. (2007) Flagellar membrane trafficking in kinetoplastids. *Parasitol Res* **100:** 205–212.

Ghosh, M., Song, X., Mouneimne, G., Sidani, M., Lawrence, D.S., and Condeelis, J.S. (2004) Cofilin promotes actin polymerization and defines the direction of cell motility. *Science* **304:** 743–747.

Gull, K. (2003) Host–parasite interactions and trypanosome morphogenesis: a flagellar pocketful of goodies. *Curr Opin Microbiol* **6:** 365–370.

Hawkins, M., Pope, B., Maciver, S.K., and Weeds, A.G. (1993) Human actin depolymerizing factor mediates a pH-sensitive destruction of actin filaments. *Biochemistry* **32:** 9985–9993.

Hill, K.L. (2003) Biology and mechanism of trypanosome cell motility. *Eukaryot Cell* **2:** 200–208.

Ismach, R., Cianci, C.M., Caulfield, J.P., Langer, P.J., Hein, A., and McMahon-Pratt, D. (1989) Flagellar membrane and paraxial rod proteins of *Leishmania*: characterization employing monoclonal antibodies. *J Protozool* **36:** 617–624.

Kapoor, P., Sahasrabuddhe, A.A., Kumar, A., Mitra, K., Siddiqui, M.I., and Gupta, C.M. (2008) An unconventional form of actin in protozoan hemoflagellate. *Leishmania J Biol Chem* **283:** 22760–22773.

Kohl, L., Robinson, D., and Bastin, P. (2003) Novel roles for the flagellum in cell morphogenesis and cytokinesis of trypanosomes. *EMBO J* **22:** 5336–5346.

Kozminski, K.G., Johnson, K.A., Forscher, P., and Rosenbaum, J.L. (1993) A motility in the eukaryotic flagellum unrelated to flagellar beating. *Proc Natl Acad Sci USA* **90:** 5519–5523.

Landfear, S.M., and Ignatushchenko, M. (2001) The flagellum and flagellar pocket of trypanosomatids. *Mol Biochem Parasitol* **115:** 1–17.

Maga, J.A., and LeBowitz, J.H. (1999) Unravelling the kinetoplastid paraflagellar rod. *Trends Cell Biol* **9:** 409–413.

Maga, J.A., Sherwin, T., Francis, S., Gull, K., and LeBowitz, J.H. (1999) Genetic dissection of the *Leishmania* paraflagellar rod, a unique flagellar cytoskeleton structure. *J Cell Sci* **112:** 2753–2763.

Mattila, P.K., Quintero-Monzon, O., Kugler, J., Moseley, J.B., Almo, S.C., Lappalainen, P., and Goode, B.L. (2004) A high affinity interactions with ADP-actin monomers underlies the mechanism and in vivo function of Srv2/ cyclase-associated protein. *Mol Biol Cell* **15:** 5158–5171.

Minoura, T.K. (2005) Impaired flagellar regeneration due to uncoordinated expression of two divergent actin genes in *Chlamydomonas*. *Zool Sci* **22:** 571–577.
Muto, E., Masaki, E., Masafumi, H.C., and Kamiya, R. (1994) Immunological detection of actin in the 14s ciliary dynein of *Tetrahymena*. *FEBS Lett* **343:** 173–176.
Nayak, R.C., Sahasrabuddhe, A.A., Bajpai, V.K., and Gupta, C.M. (2005) A novel homologue of coronin colocalizes with actin in filament-like structures in *Leishmania*. *Mol Biochem Parasitol* **143:** 152–164.
Okabe, S., and Hirokawa, N. (1989) Incorporation and turnover of biotin labeled actin microinjected into fibroblastic cells: an immunoelectron microscopic study. *J Cell Biol* **109:** 1581–1595.
Ono, S. (2007) Mechanism of depolymerization and severing of actin filaments and its significance in cytoskeletal dynamics. *Int Rev Cytol* **258:** 1–82.
Ono, S., and Benian, G.M. (1998) Two *Caenorhabditis elegans* actin depolymerizing factor/cofilin proteins, encoded by the unc-60 gene, differentially regulate actin filament dynamics. *J Biol Chem* **273:** 3778–3783.
Ono, S., Mohri, K., and Ono, K. (2004) Microscopic evidence that actin interacting protein 1 activity disassembles actin depolymerizing factor/ cofilin bound actin filaments. *J Biol Chem* **279:** 14207–14212.
Pan, J., Wang, Q., and Snell, W.J. (2005) Cilium-generated signaling and cilia-related disorders. *Lab Invest* **85:** 452–463.
Pardee, J.D., and Spudich, J.A. (1982) Purification of muscle actin. *Methods Cell Biol* **24:** 271–289.
Pazour, G.J., Wilkerson, C.G., and Witman, G.B. (1998) A dynein light chain is essential for the retrograde particle movement of intraflagellar transport (IFT). *J Cell Biol* **141:** 979–992.
Pazour, G.J., Dickert, B.L., and Witman, G.B. (1999) The DHC1b (DHC2) isoform of cytoplasmic dynein is required for flagellar assembly. *J Cell Biol* **144:** 473–481.
Pollard, T.D., and Borisy, G.G. (2003) Cellular motility driven by assembly and disassembly of actin filaments. *Cell* **112:** 453–465.
Porter, M.E., Bower, R., Knott, J.A., Byrd, P., and Dentler, W. (1999) Cytoplasmic dynein heavy chain 1b is required for flagellar assembly in *Chlamydomonas*. *Mol Biol Cell* **10:** 693–712.
Quarmby, L.M., and Parker, J.D. (2005) Cilia and the cell cycle. *J Cell Biol* **169:** 707–710.
Ralston, K.S., and Hill, K.L. (2008) The flagellum of *Trypanosoma brucei*: new tricks from an old dog. *Int J Parasitol* **38:** 869–884.
Reisler, E. (1993) Actin molecular structure and function. *Curr Opin Cell Biol* **3:** 41–47.
Rosenbaum, J.L. (2003) Organelle size regulation: length matters. *Curr Biol* **13:** R506–R507.
Rosenbaum, J.L., and Witman, G.B. (2002) Intraflagellar transport. *Nat Rev Mol Cell Biol* **3:** 813–825.
Ross, J.L., Ali, M.Y., and Warshaw, D.M. (2008) Cargo transport: molecular motors navigate a complex cytoskeleton. *Curr Opin Cell Biol* **20:** 41–47.
Sahasrabuddhe, A.A., Bajpai, V.K., and Gupta, C.M. (2004) A novel form of actin in *Leishmania*: molecular characterization, subcellular localisation and association with subpellicular microtubules. *Mol Biochem Parasitol* **134:** 105–114.
Santrich, C., Moore, L., Sherwin, T., Bastin, P., Brokaw, C., Gull, K., and LeBowitz, J.H. (1997) A motility function for the paraflagellar rod of *Leishmania* parasites revealed by PFR-2 gene knockouts. *Mol Biochem Parasitol* **90:** 95–109.
Sheterline, P., and Sparrow, J.C. (1994) Actin. *Protein Profile* **1:** 1–121.
Signor, D., Wedaman, K.P., Orozco, J.T., Dwyer, N.D., Bargmann, C.I., Rose, L.S., and Scholey, J.M. (1999) Role of a class DHC1b dynein in retrograde transport of IFT motors and IFT raft particles along cilia, but not dendrites, in chemosensory neurons of living *Caenorhabditis elegans*. *J Cell Biol* **147:** 519–530.
Snell, W.J., Pan, J., and Wang, Q. (2004) Cilia and flagella revealed: from flagellar assembly in *Chlamydomonas* to human obesity disorders. *Cell* **117:** 693–697.
Theriot, J.A. (1997) Accelerating on a treadmill: ADF/cofilin promotes rapid actin filament turnover in the dynamic cytoskeleton. *J Cell Biol* **136:** 1165–1168.
Wicks, S.R., de Vries, C.J., van Luenen, H.G., and Plasterk, R.H. (2000) CHE-3, a cytosolic dynein heavy chain, is required for sensory cilia structure and function in *Caenorhabditis elegans*. *Dev Biol* **221:** 295–307.
Wiese, M., Kuhn, D., and Grunfelder, C.G. (2003) Protein kinase involved in flagellar-length control. *Eukaryot Cell* **2:** 769–777.
Yanagisawa, H., and Kamiya, R. (2001) Association between actin and light chains in *Chlamydomonas* flagellar inner-arm dyneins. *Biochem Biophy Res Comm* **288:** 443–447.

Supporting information

Additional supporting information may be found in the online version of this article.

Please note: Wiley-Blackwell are not responsible for the content or functionality of any supporting materials supplied by the authors. Any queries (other than missing material) should be directed to the corresponding author for the article.